Contemporary Mathematics
https://ojs.wiserpub.com/index.php/CM/

Research Article

Classification of Multiple Abnormalities for X-Ray Images with Deep-Learning-Based Framework

Ahmad Hoirul Basori[1*], Sami Alesawi[1], Andi Besse Firdausiah Mansur[1], Purbandini P[2,3], Anas W. Abulfaraj[1], Sharaf J. Malebary[1]

[1] Faculty of Computing and Information Technology in Rabigh, King Abdulaziz University, Rabigh, Saudi Arabia
[2] Information Systems-Faculty of Science and Technology, Airlangga University, Surabaya, Indonesia
[3] Robotics and Artificial Intelligence Engineering-Faculty of Technology Advance and Multidiscipline, Airlangga University, Surabaya, Indonesia
E-mail: abasori@kau.edu.sa

Received: 15 September 2025; **Revised:** 23 October 2025; **Accepted:** 24 November 2025

Abstract: Obtaining an early and accurate diagnosis of pneumonia is crucial for enhancing the cure rate and reducing the mortality rate. The interpretation of chest X-Rays is contingent upon the physician's experience, potentially resulting in bias and inaccurate diagnosis. A lot of previous studies focused on the improving the classification result as well as the quality of digital Chest X-Ray datasets. This study area has promise for future advancement, focusing on the classification of chest radiographs. To enhance the Chest Radiographs dataset of patients with lung disease, we proposed employing a multistage deep transfer learning technique that integrates an updated Generative Adversarial Network (GAN). A recommendation was given, and this was one of them. The proposal encompasses the execution of multi-stage transfer learning, to be achieved by the utilization of Inception V3 and Xception, respectively. The classification findings demonstrate a high level of competence, featuring an F1 score of 98.97%, an accuracy rate of 99.14%, a precision rate of 98.80%, a recall rate of 98.34%, and an accuracy rate of 99.14%. Future studies may focus on enhancing dataset quality and investigating methods to facilitate transfer learning by utilizing alternative combinations of learning models. Both of these focal areas present potential opportunities for future research. The ultimate objective of this research is to establish a society characterized by optimal health and well-being. This will be achieved by enhancing the healthcare system in alignment with Saudi Vision 2030.

Keywords: classification, abnormalities, Deep Convolutional Generative Adversarial Network (DCGAN), chest radiograph images, lung disease detection, data augmentation

MSC: 68T07, 68T45

1. Introduction

Artificial intelligence that is capable of deep learning has opened up new opportunities for medical image processing. This technology has the potential to be utilized in an efficient manner for the detection and diagnosis of lung diseases such as pneumonia, asthma, or COVID-19 [1]. Furthermore, when it is combined with XceptionNet and GoogleNet,

DOI: https://doi.org/10.37256/cm.7220268631

the ensemble technique comes into play as one of the options for the instant detection of COVID-19 [2]. When doing an analysis of the X-Ray pictures, the researcher applied multilayer characteristics with depth-wise [3]. The others, on the other hand, suggested automatic disease detection through the utilization of a tailored median filter [4]. The other researcher concentrated on utilizing Electromagnetic (EM) diagnostics for cultural assets, integrating Machine Learning (ML) and Deep Learning (DL) to analyze data and enhance conservation strategies. This method can be integrated with various approaches for chest X-Rays, as alternative image sources may include Magnetic Resonance Imaging (MRI) images, which are based on electromagnetic physics [5].

The other researcher used ensemble transfer learning approaches based on radiographs photos in deep learning frameworks using two models [6]. In addition, AlexNet Model is also applied by other researchers in order to find abnormalities in radiological images and classify them as either normal, pneumonia, or COVID-19 respectively [7]. Some facts on infections are displayed in the previous statistic. For instance, there are roughly 801,000 infections that have been reported in Saudi Arabia, and these infections have caused approximately 9,223 deaths [8, 9]. After doing a thorough examination of radiograph images, a new option has shown itself to investigate the chronic level of COVID-19. This is because the density of images changes depending on whether the patient is infected or healthy. Moreover, it can be utilized for the purpose of forecasting the progression of the disease towards other organs [10, 11].

1.1 *The motivation of research study*

Despite a significant decline in COVID-19 instances, other pulmonary diseases such as pneumonia, lung cancer, Chronic Obstructive Pulmonary Disease (COPD), and Tuberculosis (TB) continue to affect individuals globally. Consequently, an alternate detection and classification method utilizing deep learning is essential for assisting physicians in achieving improved accuracy and expedited diagnostic results. Some studies continue to investigate the diagnosis of pneumonia from X-Ray images of the chest utilizing Yolo [12], While different researchers concentrated on rebuilding chest X-Ray picture segmentation and employing artificial intelligence analysis of chest radiographs to anticipate significant adverse outcomes in patients [13, 14].

In order to make a comparison between the picture of a healthy person and the image of a sick person, the uncertainty factor of the image can be utilized. The created image has the potential to enhance the size of the dataset, which will allow for the training to be carried out with an adequate amount of data [15]. There is also the possibility of using bidirectional with Long Short-Term Memory (LSTM) for the purpose of autonomously detecting the coronoa virus within the lung. There is also the possibility of determining the severity of the disease through the use of image processing by comparing the gray level intensity of photographs [16, 17]. Figure 1 is a representation of an example of radiograph images that have been infected with pneumonia, COVID-19, and tuberculosis.

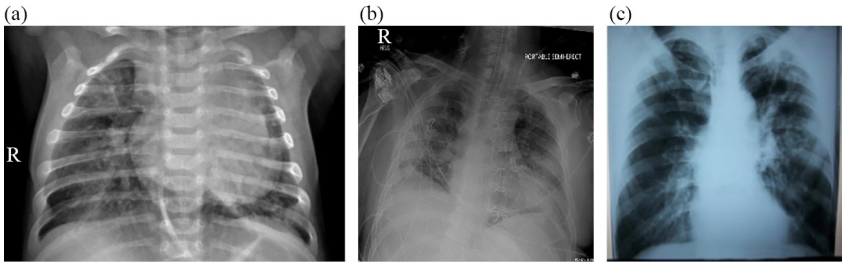

Figure 1. Sample of lung X-Ray images with various disease. (a) COVID-19; (b) Pneumonia; (c) Tuberculosis

The design of research that identifies abnormalities of lung images of patients for initial screening. The other researcher also identified COVID-19 from cough sounds using Linear Regression (LR) and Support Vector Machine (SVM). The Artificial Neural Network (ANN) and Random Forest (R.F.) are also being used for analyzing the pattern of cough and then identifying the severity of the patient's respiratory disease [18]. Disease like asthma and cough can be observed using Wigner distribution approaches in a quiet environment [18]. Another research utilizing the limited public

dataset for classifying coronavirus patients from the healthy one. They train small datasets by using two-step transfer learning design [19]. In their first step, a large pneumonia dataset is processed with pre-trained Deep Residual Network. The outcome for coronavirus diagnose in pneumonia-infected and non-infected X-Ray photos is satisfying.

Collecting medical photos is a costly and tiresome that need verification from the expert and competent person [20]. Convolutional Neural Networks (CNNs) are able to carry out the work because they have a large number of parameters that can be fine-tuned. This is the reason for their superior performance. As a result, the results of recognition and detection may obtain higher results, despite the fact that the dataset is limited [21–23]. X-Ray images is rather challenging to gather and can be costly for it need professionals and skillful person [24]. During the initial phase of the coronavirus's transmission, it was extremely challenging to gather the image dataset from patients because hospitals were primarily concerned with maintaining patient satisfaction. As a result, one of the methods that is required is one that may be used to increase the picture dataset by automatically generating an X-Ray image dataset. Image processing is also capable of transforming the image, improving its quality, and correcting any distortions that may have been there.

1.2 *The research contribution of the proposed framework*

Lung illness continues to affect a significant portion of the global population. A novel framework is required for automating the detection of lung diseases with enhanced results and precision. This statement justifies the principal contribution of our proposed framework to chest X-Ray illness categorization with detailed contributions outlined below:

• Enhancing the Quality of X-Ray Datasets via the Application of Deep Convolutional Generative Adversarial Network (DCGAN) and Enhanced DCGAN.

• In this study, we propose a multistage transfer learning approach that aims to enhance training accuracy by using the knowledge acquired by Inception V3 and Xception models.

• The K-fold cross-validation technique is commonly employed to partition the dataset into training and testing sets in order to enhance accuracy.

The structure of the paper is elaborated as follows: Chapter 1 centers on the latest knowledge and the impetus underlying the study. Chapter 2 give a summary of relevant research conducted on the use of artificial intelligence for lung illness diagnostics. Chapter 3 includes related works and proposed method. Chapter 4 includes research results and discussion of the results. Also, it assesses the implementation of the suggested framework and benchmarking with related research. Lastly, Chapter 5 includes the research conclusions.

2. Related works

The latest method of image enhancement competent of overwhelming common data amplification. previous researcher methods is Generative Adversarial Network (GAN). GAN use two elements, $G(z)$-$D(x)$, which has its own function. The purpose of $G(z)$ is to generate a trustworthy replica of the dataset by making use of a certain distinction., and $D(x)$ responsible to compute it [24]. A person who is infected with the coronavirus may have symptoms that are comparable to those of the flu and fever. Yet, serious case shows difficult to breathe, the organ failure or even death [25, 26]. As a result of the tremendous rate at which the coronavirus spread, a number of countries have been confronted with major problems in their healthcare systems. These problems are mostly the result of the difficulty in managing large numbers of patients at the same time. As a result of the rapid depletion of test kits and ventilators, the majority of nations have implemented lockdown policies, severely prohibited meetings, and demanded that everyone stay at home [27, 28]. Researchers found that the patient's lungs with coronavirus infection showed a visible mark of ground-glass opaqueness, darker than the surrounding area, and pessimistic COVID-19 persons [29, 30]. Therefore, scientists put immense faith in using Chest Radiograph images for COVID-19 detection and analysis and further action toward the patient. In the real world, analysing many cases instantaneously is needed to overcome the staff and testing kit limitations. Therefore, Image-based detection through X-Ray images has significant potential to help hospitals and teams easily detect the infected patient. X-Ray machine is primarily available at most of health facilities, and they are more familiar radiograph than the latest testing kit [29, 30]. Pneumonia usually diagnose using X-Rays, however its rather hard to discriminate chest disease

caused by pneumococcal pneumonia or coronavirus [31]. Therefore, deep learning with artificial intelligence will provide precise, inexpensive and fast results could help COVID-19 diagnose [32]. With Mask_Region-based Convolutional Neural Network (RCNN), detecting the disease on X-Ray photos could be more efficient and accurate by knowing the type and severity by patterns [33]. A number of researchers are still concentrating their efforts on identifying and analyzing COVID-19 with a high degree of precision by employing the layered composite method employing radiograph photographs and lung computed tomography scans [7]. In addition, they utilized a variety of methods, including layered design of LSTM-learning for the evaluation of coronavirus patient treatment, Bi-LSTM-Network, and metaheuristic-blend for the diagnosis of coronavirus using lung radiograph photographs[20, 34, 35].

3. Material and methods

In this research, we combined an ensemble technique with a Deep Convolutional neural network to generate a generated image to enhance the dataset of Chest Radiograph images. Ian Goodfellow et al. initially proposed the fundamental concepts of Generative Adversarial Networks (GANs) [36]. Saka [37] mentions that GAN used two neural networks: a discriminator to distinguish between two images (real or fake).

3.1 *Dataset*

Previous scientists focused on binary classification for binary images using deep learning. We have collected several typical and pneumonia patient datasets from the Kaggle X-Ray dataset with various resolutions [38]. Our dataset is also supported by an additional dataset from Joseph Paul Cohen with COVID-19 samples [39]. Figure 2 demonstrate various types of X-Ray Images with certain conditions.

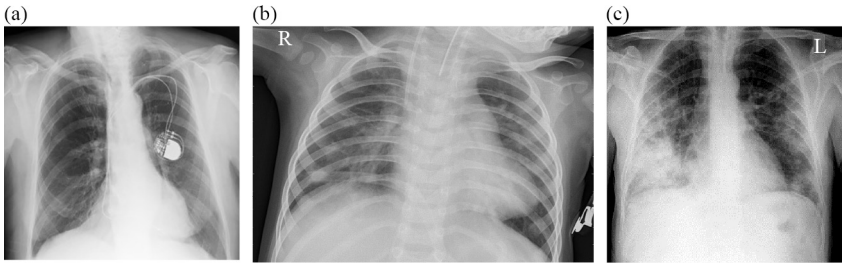

Figure 2. X-Ray images variety (a) Normal, (b) Pneumonia, (c) COVID-19

3.2 *GAN*

The generator and the discriminator are the primary components that are involved in the production of images. Generative Adversarial Network (GAN) is capable of generating images based on the characteristics of the original images. These two components are working together to collaborate in order to improve the overall quality of the photographs that are generated [40]. In addition, the other researcher is concentrating on DCGAN in order to enhance the quality of the X-Ray images that are created [41]. The diagram of GAN is clearly illustrated in Figure 3.

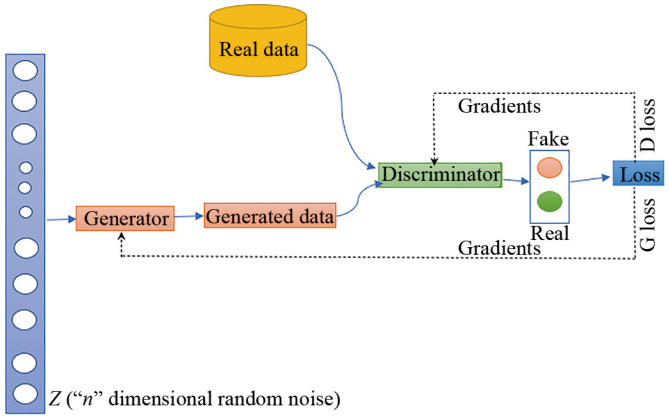

Figure 3. GAN-diagram [40]

A unique adjustment of the upper and lower limit of such network elements is required in order to activate generator and discriminator networks, which are required for the training of GAN [41]. This process is shown in Equation (1) [42].

$$\frac{\min}{G}\frac{\max}{D}V_{GAN}(D,\ G) = \mathbb{E}_{x\sim p_{data}(x)}\left[logD(x)\right] + \mathbb{E}_{z\sim p_z(z)}\left[\log\left(1-D(G(z))\right)\right]. \tag{1}$$

$\mathbb{E}_{x\sim p_{data}(x)}$ is the supposed value for actual instances while $\mathbb{E}_{z\sim p_z(z)}$ is the supposed value of fake instances. $p_z(z)$ a value that randomly allocated. $G(z)$ is the generator function which is responsible for mapping the data into space, x is original data, and $D(x)$ is the probability of actual data (x), not the generated one.

3.3 *Improved DCGAN*

The DCGAN has both a discriminator and generator that has drawbacks when dealing with min-max adjustment. Therefore, to improve the DCGAN, we adopt the algorithm proposed by Liu et al. [43] to handle gradient disappearance. Initially, the minimum cross-entropy needs to be calculated for discriminator D under the generator G. This function is calculated using Equation (2).

$$Entropy(D) = E_{x\sim P_{data}}\log\left[D(x)\right] - E_{Z\sim P_z}\log\left[1-D\left(G(Z)\right)\right]. \tag{2}$$

Where $\log\left[D(x)\right]$ is used for evaluating the sample data, where $\log\left[1-D\left(G(Z)\right)\right]$ correspond to the reasoning of created sample data. The closeness of sample data distribution is determined by discriminator Pdata and data distribution generated by GPG (x), and x is a sample from the actual data, refer to Equation (3).

$$Entropy\left(\theta_D,\ \theta_G\right) = -\int_x P_{data}(x)\log\left(D(x)\right)dx - \int_z P_z(Z)\log\left(1-D\left(G(Z)\right)\right)dz$$

$$= \int_x \left[P_{data}log(D(x) + P_G(x)log(1-D(x))\right]dx. \tag{3}$$

Due to the data and generator being predefined, they can be treated as constant values. Therefore, the generator and data can be substituted. Refer to Equation (4).

$$f(D) = c_1 \log D + c_2 \log(1 - D). \tag{4}$$

If $f(D) = 0$ in (1), the maximum point can calculated as depicted in Equation (5):

$$D*(x) = \frac{P_{data}(x)}{P_{data}(x) + P_G(x)}. \tag{5}$$

The further step is to adjust the Discriminator D. Therefore, the optimisation for generator G is computed with Equation (6).

$$V(G,\ D) = E_{x\sim p_{data}} \log D(x) +\ E_{x\sim p_G} \log\left[1 - D(x)\right]. \tag{6}$$

By referring to Equation (2), the $D*$ gives $V(G,\ D)$ the optimal solution for the generator can be computed through Equation (7).

$$\begin{aligned} \min_G V(G,\ D) &= V(G,\ D*) \\ &= E_{x\sim} P_{data}(x) \left[\log \frac{P_{data}(x)}{P_{data}(x)}\right] + E_{x\sim} P_G(x) \left[\log \frac{P_{data}(x)}{P_{data}(x) + P(G)}\right]. \end{aligned} \tag{7}$$

During the program running, the system will train the discriminator once generator D is fixed. It will be continued with training Generator G. The iteration process will be continued until optimisation training $P_{data} = PG$, which shows that optimisation is reached.

3.4 *Xception convolutional neural network*

The Convolution Neural Network (CNN) is a feed-forward neural network capable of learning by itself through kernel optimisation. According to Wu, mathematically, the convolution can be expressed as Equation (8) [44]:

$$yi^{i+1},\ ji^{i+1},\ d = \sum_{i=0}^{H} \sum_{j=0}^{W} \sum_{d^l}^{D^l} f_{i,\ j,\ d^l,\ d}\ x^l_{i^{l+1}+i,\ j^{l+1}+j,\ d^l}. \tag{8}$$

Equation (8) will be repeated for all $0 \le d \le D = D^{l+1}$, for any spatial location $i^{l+1},\ j^{l+1}$ that satisfying $0 \le i^{l+1} < H^l - H + 1 = H^{l+1},\ 0 \le j^{l+1} < W^l - W + 1 = W^{l+1}$. The element $x^l_{i^{l+1}+i,\ j^{l+1}+j,\ d^l}$ Indicates a component that is pointed by triplet $(i^{l+1} + i,\ j^{l+1} + j,\ d^l)$.

The final convolution result will be computed by $\varnothing x^1$ is B^T:

$$vec(y) = vec\left(x^{l+1}\right) = vec\left(\varnothing\left(x^l\right) F\right) \tag{9}$$

$vec(\mathbf{y}) \in \mathbb{R}^{H^{l+1}W^{l+1}D}$, $\varnothing\left(x^l\right) \in \mathbb{R}^{\left(H^{l+1}W^{l+1}\right)x(HWD^l)}$, and $F \in \mathbb{R}^{(HWD^l)xD}$. The matrix multiplication $\varnothing\left(x^l\right)F$ will generate a matrix with size $H^{l+1}W^{l+1}xD$. This vectorisation is a result of $\mathbb{R}^{\left(H^{l+1}W^{l+1}\right)D}$.

According to the chain rule, the convolution based on backward propagation will be computed by Equation (10).

$$\frac{\partial z}{\partial (vec(F))^T} = \frac{\partial z}{\partial (vec(Y)^T)} \frac{\partial vec(\mathbf{y})}{\partial (vec(F)^T)}. \tag{10}$$

The first part in Right Hand Side (RHS) is already computed in the layer $l+1$, which is $\frac{\partial z}{\partial (vec(x^{l+1}))^T}$, so the second part will be computed as Equation (11):

$$\frac{\partial vec(\mathbf{y})}{\partial (vec(F))^T} = \frac{\partial (I \otimes \varnothing(x^l) Vec(F))}{\partial (vec(F)^T)} = I \otimes \varnothing\left(x^l\right). \tag{11}$$

If we used the fact $\frac{\partial Xa^T}{\partial a} = X$ or $\frac{\partial Xa}{\partial a^T} = X$, then it will lead to equation (12).

$$\frac{\partial z}{\partial (vec(F))^T} = \frac{\partial z}{\partial (vec(Y)^T)} \left(I \otimes \varnothing\left(x^l\right)\right). \tag{12}$$

By applying transpose, then equation will transform into Equation (13)-(16).

$$\frac{\partial z}{\partial (vec(F)} = \left(I \otimes \varnothing\left(x^l\right)\right)^T \frac{\partial z}{\partial vec(\mathbf{y})} \tag{13}$$

$$= \left(I \otimes \varnothing\left(x^l\right)\right)^T vec \frac{\partial z}{\partial \mathbf{Y}} \tag{14}$$

$$= vec\left(\varnothing\left(x^l\right)\right)^T \frac{\partial z}{\partial \mathbf{Y}} I \tag{15}$$

$$= vec\left(\varnothing\left(x^l\right)\right)^T \frac{\partial z}{\partial \mathbf{Y}}. \tag{16}$$

The final equation can be presented in Equation (17) by applying the Kronecker product.

$$\frac{\partial z}{\partial \mathbf{F}} = \varnothing\left(x^l\right)^T \frac{\partial z}{\partial \mathbf{Y}}. \tag{17}$$

As part of the Convolutional Neural Network, Xception relied on extreme inception architecture that uses depth-wise separable convolution [45]. This model enlarged the initial inception block by changing the dimension into a single size (3×3) tailed by a (1×1) convolution to decrease the complexity. The effectiveness of the Xception block is because it separates channel and spatial correspondence.

In addition, the 1×1 convolution is applied to convolved output of inserting a small dimension. Subsequently, k spatial transformation is performed, where k denotes the width degree. The computation is simplified by particularly convoluting each channel near spatial axes. The advantage of Xception architecture is the utilisation of the same number of transformation segments with several channels. While traditional CNN only uses a single transformation segment. Therefore, Xception learning has increased the efficiency and performance of learning.

Figure 4 shows the Xception block architecture. The system will feed input toward pointwise convolution and then continue with output channels based on depthwise convolution. Finally, it goes into the last 1×1 convolution.

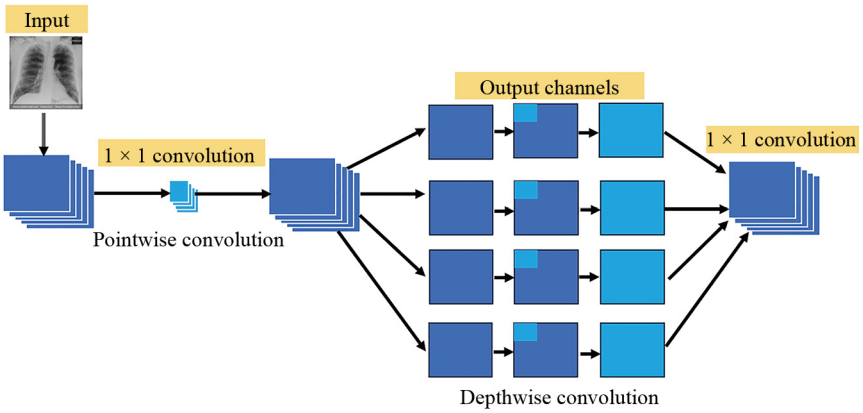

Figure 4. Xception block architecture (Chollet [45])

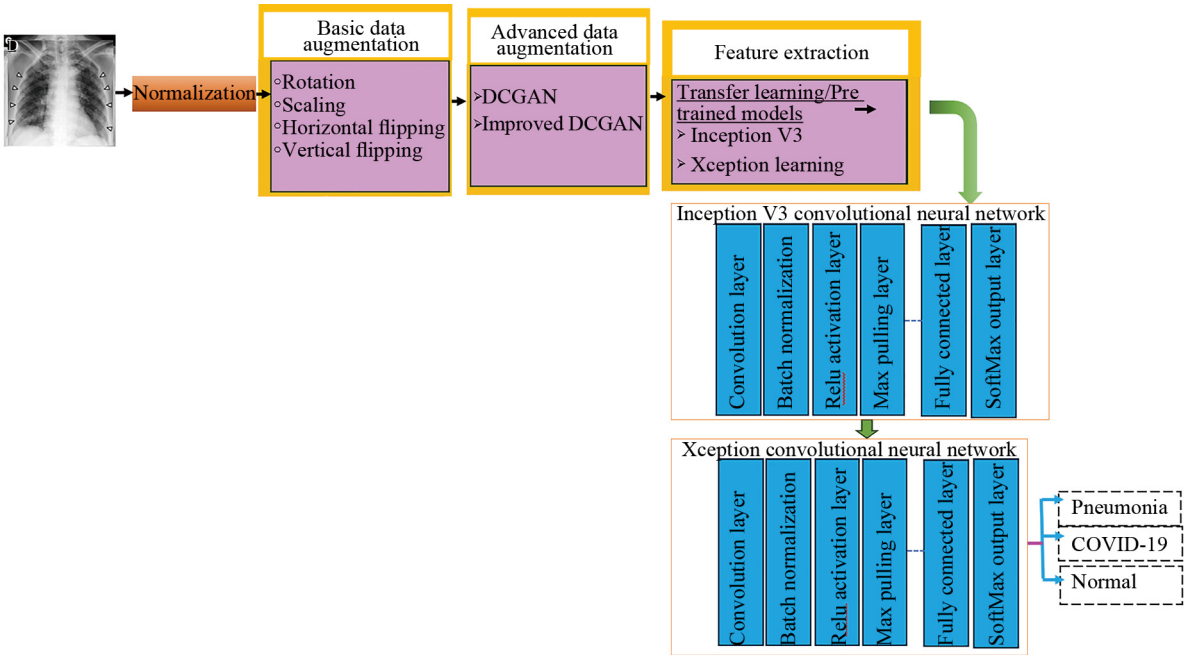

Figure 5. Proposed methodology for improved DCGAN and inception-Xception architecture

The proposed method is broken down into its component parts and depicted in Figure 5. Following the initial scaling of the image to dimensions of 288 by 288 pixels, it will then be tossed into the training process. Following that, the primary data augmentation, which includes changes such as rotation, scaling, and horizontal and vertical flipping, is

implemented. Following that, the process will be maintained with the help of the Xception convolutional neural networks and the Inception v3 transfer learning model.

There are four main steps in the data augmentation and transfer learning process. The detailed algorithm is depicted in Algorithm 1.

Algorithm 1 Data augmentation & multistage transfer learning classification.

Input: Chest Radiograph dataset $I(x,\ y)$.

Step 1: Initial Processing, change image to grayscale-mode, use normalisation. $I:\{\mathbb{X}\subseteq\mathbb{R}^n\}\rightarrow\{Min,\ \ldots,\ Max\}$ Become. $I_N:\{\mathbb{X}\subseteq\mathbb{R}^n\}\rightarrow\{new\ Min,\ \ldots,\ new\ Max\}$. $I_N=(new\ Max-new\ Min)\dfrac{1}{1+e^{-\frac{I-\beta}{\alpha}}}+newMin.$

Step 2: Basic image enhancement (scale, flip, rotate).

Scale, $I(x,\ y)$, $x_{ratio}=\dfrac{old\_image.x}{new\_image.x}$.

$y_{ratio}=\dfrac{old\_image.y}{new\_image.y}$.

$I_{new}\left(floor\left(x*x_{ratio}\right),\ floor(y*y_{ratio})\right)$.

Horizontal flip, $I_{new}(width-x-1,\ y)$.

Rotation $I_{new}=(x_r,\ y_r)$.

$$x_r=(x-center\_x)*\cos(angle)-(y-center\_y)*\sin(angle)+center\_x,$$

$$y_r=(x-center\_x)*\sin(angle)+(y-center\_y)*\cos(angle)+center\_y.$$

Step 3: Expanded dataset Enhancement (Improved-DCGAN).

Compute the expected value of real $\mathbb{E}_{x\sim p_{data}(x)}$ and fake instance.

$\mathbb{E}_{z\sim p_z(z)}$ using equation (1).

Manage the gradient disappearance by calculating $Entropy(D)$.

Via equation (3). Then perform operations for optimisation of operator G, $V(G,\ D)$.

Step 4: The Retrieval of Characteristics.

Insert-image $I_{new}=(x_r,\ y_r)$, through CNN, calculate the output of Pixel Value $V=\dfrac{\sum_{i=1}^{q}\left(\sum_{j=1}^{q}f_{ij}d_{ij}\right)}{F}$.

Afterwards, the pixel value for convolution is presented in Equation (17). The $vec(y)$ for final convolution is processed by Equation (9).

Output: $\mathbf{I_{new}}=(\mathbf{x_r},\ \mathbf{y_r})$.

3.5 *K-fold cross-validation*

We adopt the idea of K-fold cross-validation from Opeoluwa [46]. The basic idea of k-fold cross-validation is how to train the K classifiers ($\mathbf{\Phi_1},\ \mathbf{\Phi_2},\ \mathbf{\Phi_3},\ \ldots,\ \mathbf{\Phi_k}$). Each classifier will be prepared by its own learning set $\mathbf{L_k}=\dfrac{\mathbf{D}}{\mathbf{D_k}}$, while the performance will use its testing set too: $\mathbf{T_k}=\mathbf{D_k}$. Therefore the probability can be computed by equation (18).

$$\mathbf{p}\left(\text{error};\ \Phi\right)\approx\mathbf{p}\left(\text{error};\ \mathbf{\Phi_k}\right). \tag{18}$$

To attain the impartial approximation of probability $\widehat{\mathbf{p}}(\text{error})$, the classifier Φ for the complete dataset D. So according to the basic equation for cross-validation depicted in Equation (18). Let $\mathbf{N_{jj}^{(k)}}$ Represent the number of classes from samples (ω_j) in $\mathbf{T_k}=\mathbf{D_k}$ classified as ω_j by $\mathbf{\Phi_k}$. Furthermore, the aggregate amount of class ω_j

samples in D that are classified as ω_j is described by $\mathbf{N_{jj}} = \sum_{\mathbf{K=1}}^{\mathbf{K}} \mathbf{N_{jj}^{(k)}}$. $\mathbf{N^{(k)}} = \dfrac{\mathbf{N}}{\mathbf{K}}$ is samples inside $\mathbf{T_k}$, $\mathbf{N_j^{(k)}} = \dfrac{\mathbf{N}}{\mathbf{K}}$ is number of class ω_j sample in $\mathbf{T_k} = \mathbf{D_k}$.

Then $\mathbf{N_j} = \sum_{\mathbf{K=1}}^{\mathbf{K}} \mathbf{N_j^{(k)}}$ is number of class ω_j sample in $\mathbf{D}$. The $P(\omega_j)$ is the preceding probability for class ω_j samples with $j = 1, 2, \ldots$ and $k = 1, 2, 3 \ldots K$ folds. If we consider Z a random variable for the classifier Φ trained on D, Z can be presented as Equation (19).

$$\mathbf{Z}(\mathbf{x},\ \mathbf{t}) = \begin{cases} 1 & \text{if } \Phi(\mathbf{x}) \neq \mathbf{t} \\ 0 & \text{else.} \end{cases} \tag{19}$$

If vector x and target t, with $\mathbf{E}(\mathbf{Z}) = \mathbf{P}(\Phi(\mathbf{x}) \neq \mathbf{t})$, then $\mathbf{E}(\mathbf{Z}|\omega_j) = \mathbf{P}(\Phi(\mathbf{x}) \neq \mathbf{t})\,|\omega_j = \mathbf{P}(\text{error}|\omega_j)$
Therefore, the probability can be defined as Equation (20):

$$\mathbf{P}(\text{error}) = \sum_{\mathbf{j=1}}^{\mathbf{c}} \mathbf{p}(\text{error},\ \omega_j) = \sum_{\mathbf{j=1}}^{\mathbf{c}} \mathbf{p}(\omega_j)\,\mathbf{E}(\mathbf{Z}|\omega_j). \tag{20}$$

Opeoluwa [46] simplified those equations even further become Equation (21):

$$\widehat{\mathbf{p}}(\text{error};\ \Phi_\mathbf{k}) = \sum_{\mathbf{j=1}}^{\mathbf{c}} \mathbf{p}(\omega_j)\,\frac{\mathbf{1}}{\mathbf{N_j^{(k)}}}\left(\mathbf{N_j^{(k)}} - \mathbf{N_{jj}^{(k)}}\right) \tag{21}$$

$$\widehat{\mathbf{p}}(\text{error};\ \Phi_\mathbf{k}) = \frac{\mathbf{1}}{\mathbf{K}} \sum_{\mathbf{k=1}}^{\mathbf{K}} \widehat{\mathbf{p}}(\text{error};\ \Phi_\mathbf{k}). \tag{22}$$

To obtain the Standard Error (S.E.) for unbiased S.E. of $\widehat{\mathbf{p}}(\text{error})$ can be computed through Equation (22):

$$\mathbf{SE}(\widehat{\mathbf{p}}) = \sqrt{\sum_{\mathbf{j=1}}^{\mathbf{c}} (\mathbf{p}(\omega_j))^2\,\frac{\mathbf{1}}{\mathbf{N_j}}\widehat{\mathbf{p}}_\mathbf{j}\left(\mathbf{1} - \widehat{\mathbf{p}}_\mathbf{j}\right)}$$

$$= \sqrt{\sum_{\mathbf{j=1}}^{\mathbf{c}} (\mathbf{p}(\omega_j))^2\,\frac{\mathbf{s_j^2}}{\mathbf{N_j}}}. \tag{23}$$

We do stratified K-Fold Cross-Validation with $k = 5$ for model training and assessment. The training will be conducted repeatedly using k-fold cross-validation (default: $k = 5$). Only models that attain an F1-score exceeding a specified threshold are kept; subsequently, underperforming models are eliminated before to the formation of the ensemble. The fragment code for the k-fold cross-validation is depicted in Figure 6.

```
k_fold = 5
epoch_num = 10

def train_kfold (model_name, k = k_fold, f1_threshold = 0.90, max_epochs = epoch_num, PCount = 10):
Cfold = StratifiedKFold (n_splits = k, shuffle = True, random_state = SEED)
    fold_results = [ ]
    best_models = [ ]

    label_tensor = torch.tensor (full_labels)
    class_sample_counts = torch.bincount (label_tensor)

    class_weights = 1.0/class_sample_counts.float ( )
    class_weights = class_weights/class_weights.sum ( )
    class_weights = class_weights.to (device)

for fold, (train_idx, val_idx) in enumerate(Cfold.split (np.zeros(len(full_labels))), full_labels)):
print(f"\n---Fold {fold + 1}---")
```

Figure 6. K-fold cross-validation fragment code

3.6 *Evaluation metrics*

Precision, recall, and F1-score are the measures that we have consistently used for evaluation, as they are the most frequent and typical measurements. Equation (23) and Equation (24) comprise the terms of the common parameters:

$$\text{Precision} = \frac{\text{TP}}{\text{TP} + \text{FP}'} \tag{24}$$

$$\text{Recall or True Positive Rate} = \frac{\text{TP}}{\text{TP} + \text{FN}'}. \tag{25}$$

On the other hand, the values FP., FN., TP., and TN. represent, respectively, false-positive, false-negative, true-positive, and true-negative characteristics. It is possible to compute the F1 score, which is used to evaluate the correctness of the method, by utilizing the formula (25):

$$\text{F1} = \frac{2 \times \text{Precision} \times \text{Recall}}{\text{Precision} + \text{Recall}} = \frac{2\text{TP}}{2\text{TP} + \text{FP} + \text{FN}'}. \tag{26}$$

4. Result and discussion

This section describes the proposed DCGAN-Inception V3 learning implementation details for Chest-X Ray image augmentation and classification.

4.1 *Improved data augmentation*

As described in the previous section, advanced image augmentation is performed using improved DCGAN. The dark canvas is generated at the beginning of iteration, as shown in Figure 7. Then, after hundreds of iterations, the chest image gradually appears with more acceptable quality (Figure 8).

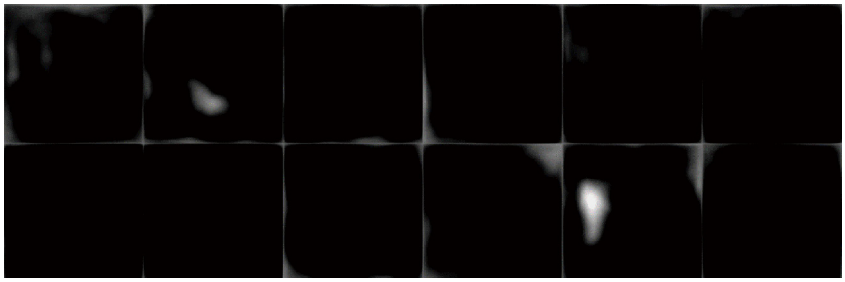

Figure 7. The initial iteration of improved DCGAN (#1st iteration improved DCGAN)

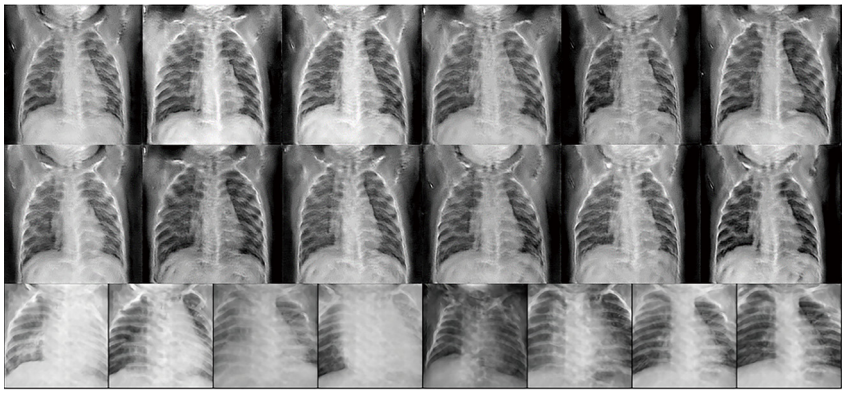

Figure 8. Chest radiograph images after the 476th iteration of improved DCGAN

Figure 8 quality generates the complete portion of the chest area, including the images of rib bone, spine bone, digestion area, etc. In Figure 9, the fluctuated loss-rate of Generator along the iteration, while the discriminator also fluctuated, but it decreased significantly after the 2,000th plus iteration.

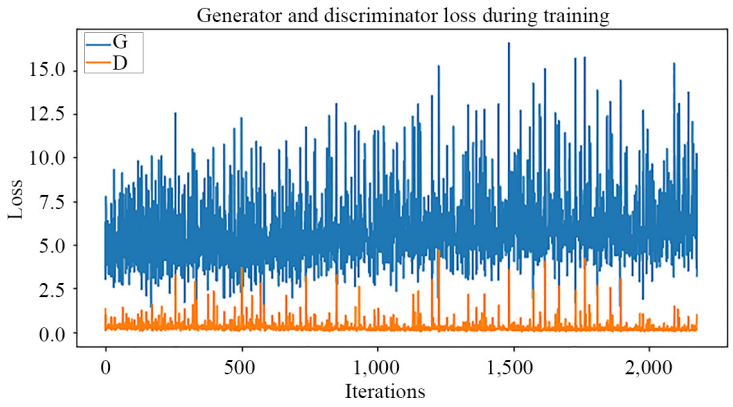

Figure 9. The loss graph for generator-discriminator

4.2 *Classification results*

The main sources of datasets are a pair of distinct sources (Cohen [39], Tabik [47], and Shuja [48]). Additionally, the dataset produced by the DCGAN and the enhanced DCGAN process is utilized for training and testing purposes. This

research framework is trained using 9,300 images categorized as non-disease (3,300), pneumonia (2,500), and COVID-19 (3,500). Subsequently, we evaluated 1,049 pictures, comprising 294 normal, 424 pneumonia, and 331 COVID-19 cases. Subsequently, the model is trained using Inception Learning V3 with a batch size of 128 for 100 epochs. Subsequently, proceed with the transfer to Xception (batch size of 256 and 100 epochs). The image size distribution depicted in Figure 10 is quantified for each sample class to contrast positive and negative examples, hence illustrating class imbalance in the data.

We use weighted binary cross-entropy loss to handle the result with false positives. If the number of one class is dominant, we can shift the bias, forcing the model to give the same weight for each categorised image, using Equation (26).

$$L_{cross-entropy}(D) = \frac{1}{6}\left(\sum_{positive\ examples} log\left(f(x_i)\right) + \sum_{negative\ examples} log\left(1 - f(x_i)\right)\right). \tag{27}$$

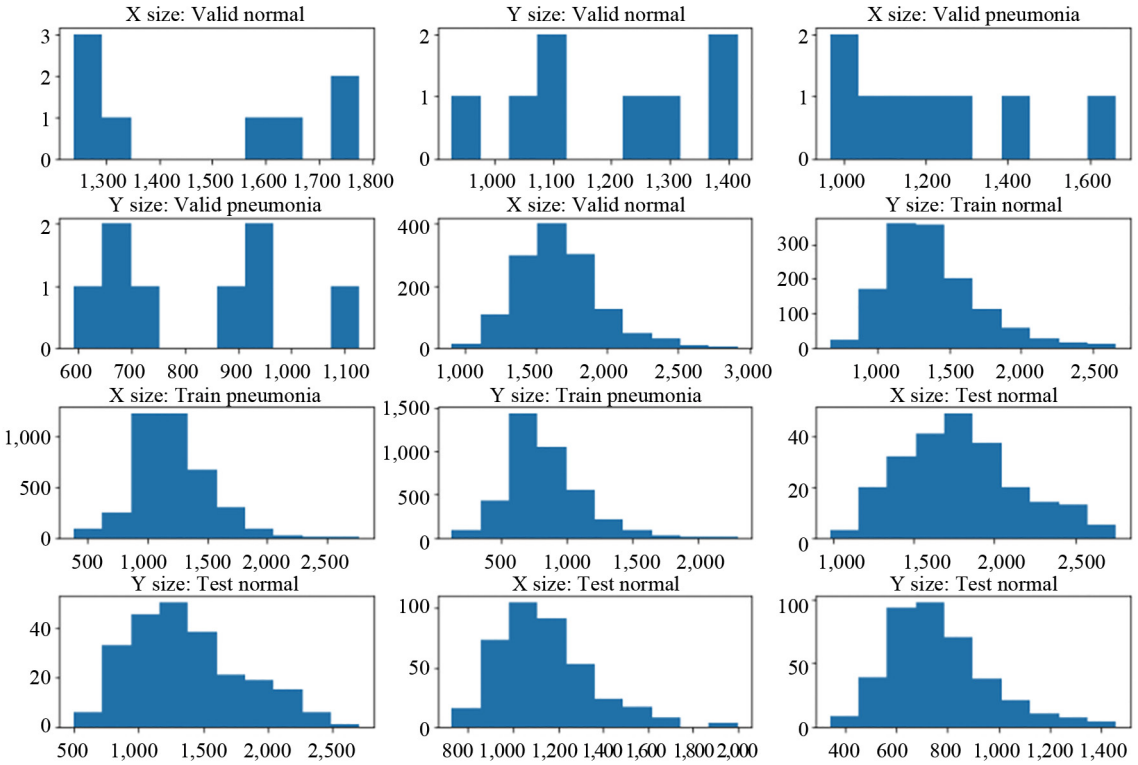

Figure 10. Class imbalance dataset

This research employ weighted binary cross-entropy loss to address the prevalence of false positives. The rationale is that, due of the abundance of X-Ray pictures depicting Pneumonia, the model assigns greater weight to erroneous classifications. We adjust this bias to compel the model to assign equal importance to normal and pneumonia images. This formulation indicates that a significant imbalance, characterized by a scarcity of negative training images (normal), will result in the loss being predominantly influenced by the negative class (normal), as depicted in Figure 11.

```
freq_neg = tot_normal_train/(tot_normal_train + tot_pneumonia_train)
freq_pos = tot_pneumonia_train/(tot_normal_train + tot_pneumonia_train)

pos_weights = np.array ([freq_neg])
neg_weights = np.array ([freq_pos])

print ('check positive weight: ', pos_weights, len (pos_weights))
print ('check negative weight: ', neg_weights)

def get_weighted_loss (pos_weights, neg_weights, epsilon=1e-7):
def weighted_loss (y_true, y_pred):
# initialize loss to zero
    loss = 0.0

    for i in range (len (pos_weights)): # we have only 1 class
    # for each class, add average weighted loss for that class
    loss + = - (K.mean ((pos_weights [i] * y_true [:, i] * K.log (y_pred [:, i] + epsilon)) +
                        (neg_weights [i] * (1-y_true [:, i]) * K.log (1-y_pred [:, i] + epsilon))))
        return loss
    return weighted_loss
```

Figure 11. Imbalance code for weighted cross-entropy

The outcome shows that the best accuracy of training and validation of recommended model are 97.90% and 99.14%, respectively. At the same time, the loss (0.0086), respectively, as shown in Figure 12.

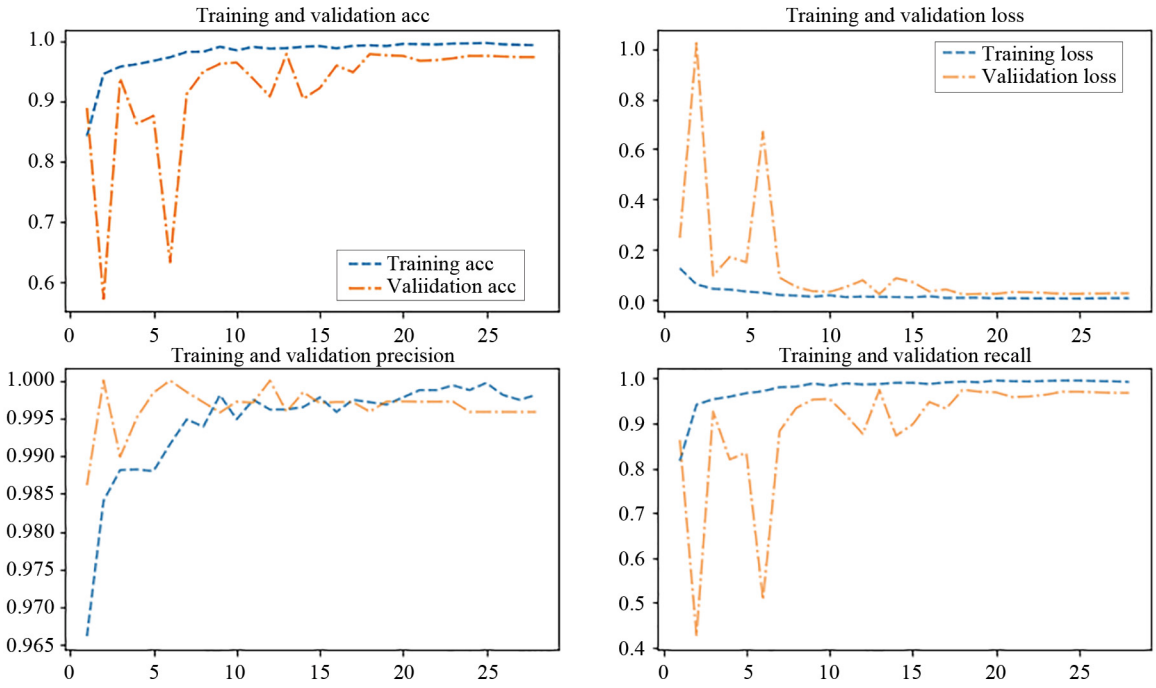

Figure 12. Accuracy-loss-validation-recall graph

The positive outcome of the training is that the recognition process is comparable to the dataset that was initially utilized. This is a very encouraging development. In terms of contrast, saturation, and the amount of noise, the visual quality of some of the data is substantially higher than that of the original dataset. All of these metrics are taken into consideration. A classification of the transfer learning (Inception v3-Xception) using the DCGAN and Improved DCGAN dataset is shown in Figure 13, which shows the outcomes of the classification.

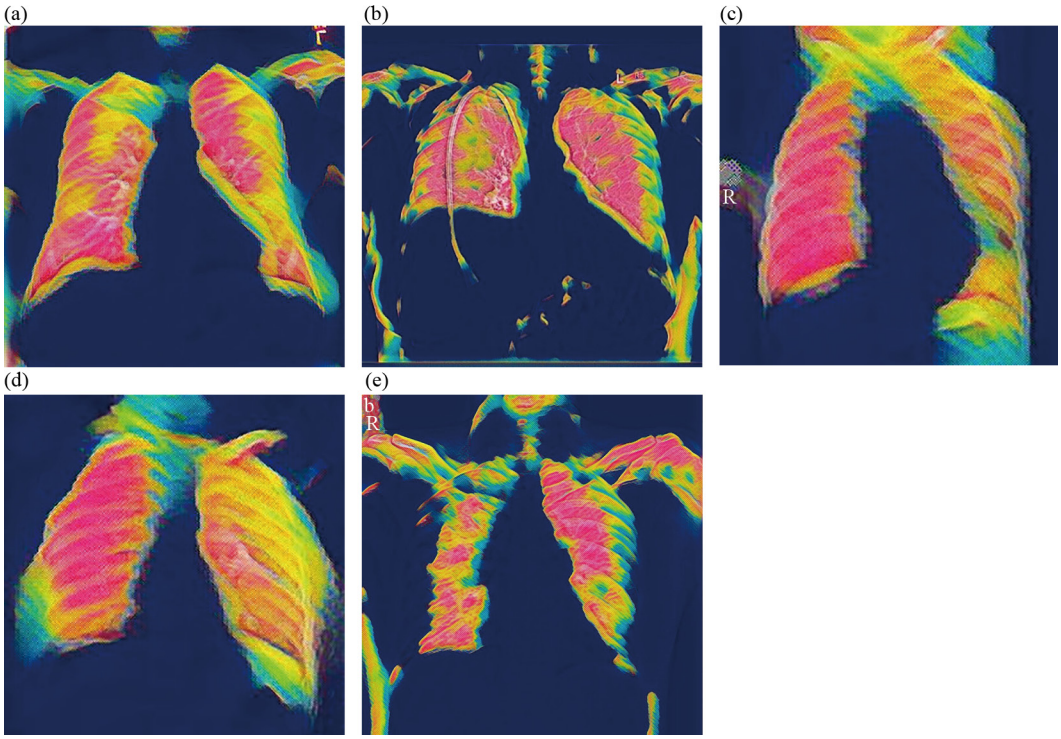

Figure 13. Classification result of three classes (Normal; Pneumonia; COVID-19). (a) Ori: COVID-19; Pred: COVID-19; (b) Ori: Normal; Pred: Normal; (c) Ori: Pneumonia; Pred: Pneumonia; (d) Ori: COVID-19; Pred: COVID-19; (e) Ori: COVID-19; Pred: COVID-19

4.3 *Performance evaluation*

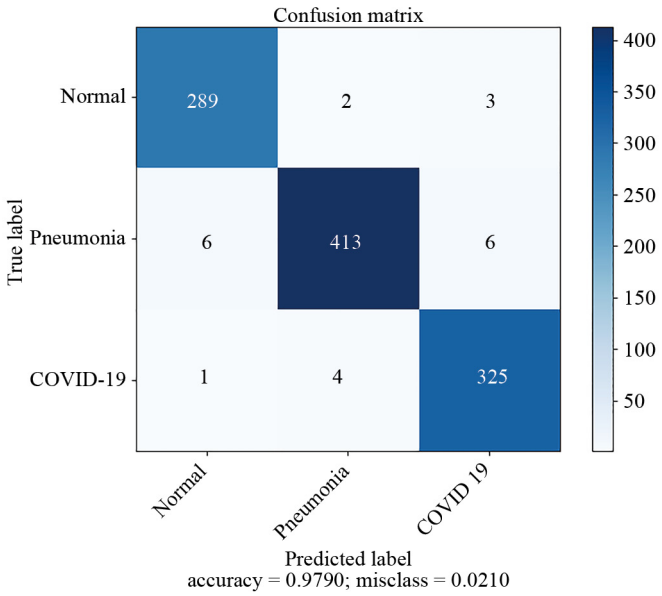

Figure 14. Confusion matrix for with inception v3 and improved DCGAN dataset

We also evaluate the performance of the proposed approach with the confusion matrix. Figure 14 depicts the scenario without transfer learning, only using an improved DCGAN dataset with an inception V3 training model. In addition, Figure 15 shows the confusion matrix of the proposed approach with transfer learning between Inceptionv3 to Xception learning.

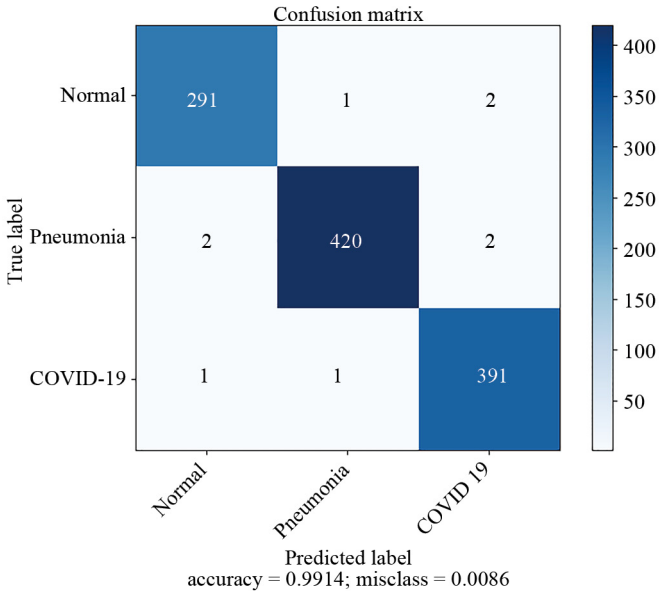

Figure 15. Confusion matrix for the proposed approach with transfer learning

We can see some accuracy improvement when the transfer learning is applied, and then accuracy changed from 97.9% to 99.1%. The proposed approach can identify around 291 normal, 420 Pneumonia, and 329 COVID-19 cases with transfer learning. The average ROC curve is shown in Figure 16.

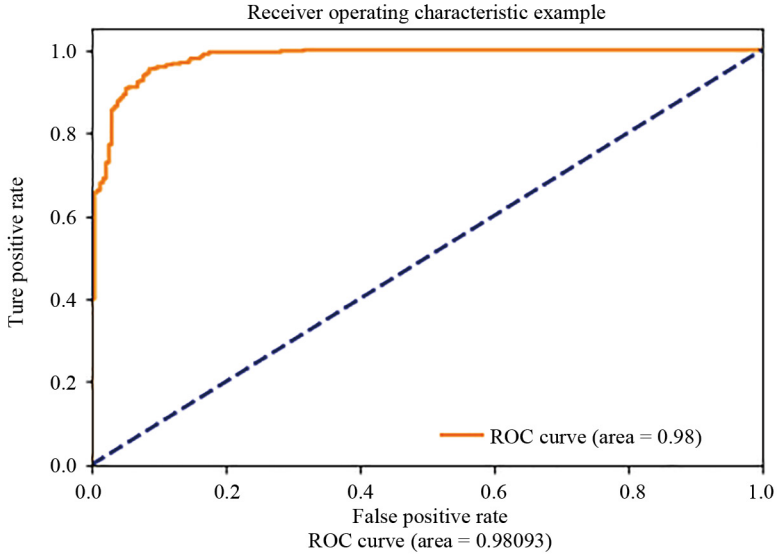

Figure 16. The ROC curve for the proposed approach

The results of the numerous testing situations are presented in Table 1, which includes: VGG19 + Original dataset, Inception V3 improved DCGAN dataset, and transfer learning (Inception V3 + Xception) + Improved DCGAN dataset. The F1-score, accuracy, precision, and recall of the individuals in question. According to the findings, the transfer learning methodology achieved a higher accuracy score than the other method, indicating that it functioned better with 99.14%, Precision (98.8%), Recall 98.34%, and F1-Score 98.97%.

Table 1. Performance analysis between three scenarios

Method	Accuracy-score	Precision-score	Recall-score	F1-score
VGG 19 + Original dataset	79.02	79.20	81.20	80.12
Inception V3 + improved DCGAN	97.90	96.9	97.17	97.72
Improved DCGAN + Transfer learning (Inception V3 + Xception)	99.14	98.80	98.34	98.97

As seen in Figure 17, the benchmarking procedure is shown together with the methods that were used in the past. Upon closer analysis, it is clear that the combination of transfer learning and the enhanced DCGAN dataset is significantly superior to the methods that were previously utilized.

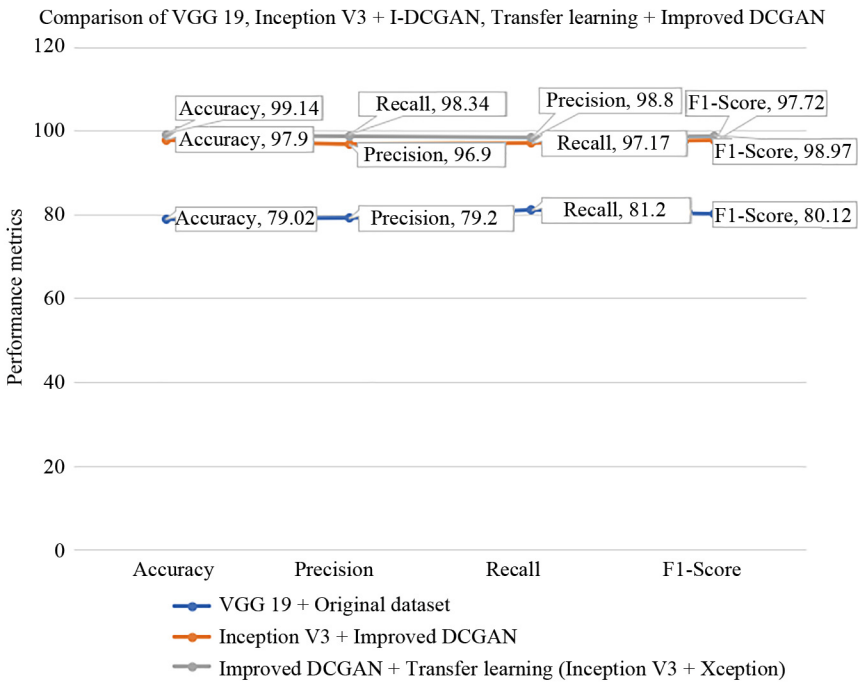

Figure 17. Performance metrics illustration of transfer learning with other approaches

4.4 *Performance comparison*

A comparison between our techniques and related works has been presented in Table 2 to show the contribution of the proposed approach.

As depicted in Table 2, there is previous work using the transfer-learning approach to classify the chest-X Ray images and gain 98.62% accuracy, which another researcher achieved with the Covinet-CNN practice. AlexNet-framework has reached 93.42% accuracy with a sensitivity of around 89.18%. The closed result performance was made by fine-tuned

Dense Net 121. Additionally, our proposed approach shows fascinating results with 98.86% accuracy, 99.9% in sensitivity score and 98.7% in recall. This result is affected by improving Chest Radiograph image quality through the improved DCGAN process. The training combination between the original & generated DCGAN data through the transfer learning (Inception V3 + Xception) learning model becomes flawless integration. The framework that has been proposed is capable of overcoming other approaches that have been taken in the past, as shown in Figure 18.

Table 2. Comparison of proposed approaches with existing works

Previous research	Image data	Methodology	Accuracy-score	Sensitivity-score	Recall-score
[49]	Chest-radiograph	Transfer learning	98.7%	95.0%	95.0%
[4]	Chest-radiograph	CNN-covinet	98.6%	95.8%	93.7%
[50]	Chest-radiograph	Transfer-learning	98.5%	94.1%	98.5%
[51]	Chest-radiograph	ResNet 34 & HRNets	97.1%	95.6%	98.4%
[52]	Chest-radiograph	AlexNet mode	94.2%	93.4%	89.1%
Proposed method	Chest radiograph & Improved chest radiograph	Transfer learning (Inception V3+ Xception)	99.1%	98.5%	98.3%

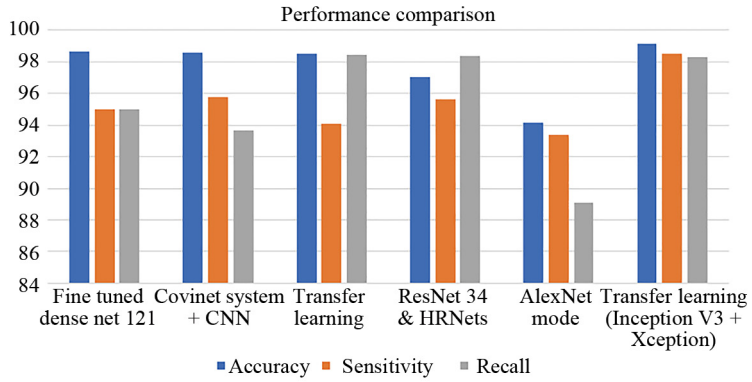

Figure 18. Performance metrics comparison with other related works

4.5 *Observations about the experiment*

Using the combination of ensemble techniques between Improved DCGAN + transfer learning, we can improve the prediction score of Chest-Radiograph data. Figure 16 depicts the proposed approach performance, showing that our improved DCGAN + multistage Transfer Learning (Inception v3 + Xception) has positively overcome the preceding research result. Table 2 demonstrate various transfer learning techniques comparison such as fine-tuned Dense Net 121, ResNet, and AlexNet. The improved method has given a promising boost toward the result. The intended method show an improvement of (accuracy-precision-recall and F1-score) by 0.45-1.7% in the average achievement of an experiment. The improvement is due to a combination of DCGAN + inception V3 and XGradient Boost. However, if we performed a comparison 1 : 1, some achievements could reach a 4.96 % improvement

5. Conclusion and future works

There are still a lot of people throughout the world who are affected by lung disease. The COVID-19 virus, which is considered to be one of the worst cases, continues to leave an indelible stamp on people's memory due to the fact that its effects are enduring. Taking this into consideration, a significant amount of research has been conducted with

the goal of simplifying the process and improving the accuracy of the findings of the detection. Computer vision and artificial intelligence have emerged as two of the most fascinating fields of research over the course of the past few years. The employment of image analysis techniques in the interpretation of chest radiographs has gained a significant degree of popularity in recent years. This is because these techniques are a valuable tool that medical professionals may utilize to enable correct diagnosis. Two primary focal areas are explored in this work. Both of these issues are important. Through the utilization of a multistage transfer learning model and an improved Deep Convolutional Generative Adversarial Network (DCGAN), the recognition process was able to achieve a higher level of accuracy. The usage of data augmentation techniques allowed for the successful completion of this task. To be more specific, the Inception V3 and Xception models were put into action, which resulted in an improvement in performance. The classification outcome that was created is worthy of being mentioned because it received a score of 99.14% for accuracy and 98.51% for sensitivity for classification. Enhancing the quality of the dataset or refining the transfer learning process by the utilization of alternative learning model combinations, such as comparison with Vision Transformers or hybrid CNN Transformer models, may be the key focus of future study endeavors. This might be realized through the utilization of alternative learning model combinations.

Acknowledgement

The authors extend their appreciation to the Deputyship for Research & Innovation, Ministry of Education in Saudi Arabia, for funding this research work through the project number "IFPRC-216-830-2020" and King Abdulaziz University, DSR, Jeddah, Saudi Arabia.

Conflict of interest

The authors declare that they have no known competing financial interests or personal relationships that could have appeared to influence the work reported in this paper.

References

[1] Kumar N, Gupta M, Gupta D, Tiwari S. Novel deep transfer learning model for COVID-19 patient detection using X-Ray chest images. *Journal of Ambient Intelligence and Humanized Computing*. 2023; 14: 469-478. Available from: https://doi.org/10.1007/s12652-021-03306-6.

[2] Qayyum A, Razzak I, Tanveer M, Kumar A. Depth-wise dense neural network for automatic COVID-19 infection detection and diagnosis. *Annals of Operations Research*. 2021; 1-21. Available from: https://doi.org/10.1007/s10479-021-04154-5.

[3] Shah FM, Joy SKS, Ahmed F, Hossain T, Humaira M, Ami AS, et al. A comprehensive survey of COVID-19 detection using medical images. *SN Computer Science*. 2021; 2: 6. Available from: https://doi.org/10.1007/s42979-021-00823-1.

[4] Lafraxo S, El Ansari M. CoviNet: Automated COVID-19 detection from X-Rays using deep learning techniques. In: *2020 6th IEEE Congress on Information Science and Technology (CiSt)*. Agadir-Essaouira, Morocco: IEEE; 2020. p.489-494. Available from: https://doi.org/10.1109/CiSt49399.2021.9357250.

[5] Piersigilli P, Citroni R, Mangini F, Frezza F. Electromagnetic techniques applied to cultural heritage diagnosis: State of the art and future prospective: A comprehensive review. *Applied Sciences*. 2025; 15: 6402. Available from: https://doi.org/10.3390/app15126402.

[6] Akram T, Attique M, Gul S, Shahzad A, Altaf M, Syed Rameez Naqvi S, et al. A novel framework for rapid diagnosis of COVID-19 on computed tomography scans. *Pattern Analysis and Applications*. 2021; 24: 951-964. Available from: https://doi.org/10.1007/s10044-020-00950-0.

[7] Jangam E, Barreto AAD, Annavarapu CSR. Automatic detection of COVID-19 from chest CT scan and chest X-Rays images using deep learning, transfer learning and stacking. *Applied Intelligence*. 2022; 52: 2243-2259. Available from: https://doi.org/10.1007/s10489-021-02393-4.

[8] Ministry of Health. *COVID-19 command and control center CCC, the national health emergency operation center NHEOC*. Available from: https://COVID-19.moh.gov.sa [Accessed 10th September 2025].

[9] Worldometer. *CoronaVirus Cases Statistics*. Available from: https://www.worldometers.info/coronavirus [Accessed 10th September 2025].

[10] Wang S, Sun J, Mehmood I, Pan C, Chen Y, Zhang Y-D. Cerebral micro-bleeding identification based on a nine-layer convolutional neural network with stochastic pooling. *Concurrency and Computation: Practice and Experience*. 2020; 32: e5130. Available from: https://doi.org/10.1002/cpe.5130.

[11] Wang S, Tang C, Sun J, Zhang Y. Cerebral micro-bleeding detection based on densely connected neural network. *Frontiers in Neuroscience*. 2019; 13: 422. Available from: https://doi.org/10.3389/fnins.2019.00422.

[12] Xie Y, Zhu B, Jiang Y, Zhao B, Yu H. Diagnosis of pneumonia from chest X-Ray images using YOLO deep learning. *Frontiers in Neurorobotics*. 2025; 19: 1576438. Available from: https://doi.org/10.3389/fnbot.2025.1576438.

[13] Chehade AH, Abdallah N, Marion JM, Hatt M, Oueidat M, Chauvet P. Reconstruction-based approach for chest X-Ray image segmentation and enhanced multi-label chest disease classification. *Artificial Intelligence in Medicine*. 2025; 165: 103135. Available from: https://doi.org/10.1016/j.artmed.2025.103135.

[14] Rhee C, Hong KJ, Kim KH, Goo JM, Hwang EJ. Artificial intelligence analysis of chest radiographs for predicting major adverse events in patients visiting the emergency department with acute cardiopulmonary symptoms. *Korean Journal of Radiology*. 2025; 26(9): 877-887. Available from: https://doi.org/10.3348/kjr.2025.0237.

[15] Zhao D, Zhu D, Lu J, Luo Y, Zhang G. Synthetic medical images using F & BGAN for improved lung nodules classification by multi-scale VGG 16. *Symmetry*. 2018; 10: 519. Available from: https://doi.org/10.3390/sym10100519.

[16] Akyol K, Şen B. Automatic detection of Covid-19 with bidirectional LSTM network using deep features extracted from chest X-Ray images. *Interdisciplinary Sciences: Computational Life Sciences*. 2022; 14: 89-100. Available from: https://doi.org/10.1007/s12539-021-00463-2.

[17] Autee P, Bagwe S, Shah V, Srivastava K. StackNet-DenVIS: A multi-layer perceptron stacked ensembling approach for COVID-19 detection using X-Ray images. *Physical and Engineering Sciences in Medicine*. 2020; 43: 1399-1414. Available from: https://doi.org/10.1007/s13246-020-00952-6.

[18] Alqudaihi KS, Aslam N, Khan IU, Almuhaideb AM, Alsunaidi SJ, Ibrahim NMAR, et al. Cough sound detection and diagnosis using artificial intelligence techniques: Challenges and opportunities. *IEEE Access*. 2021; 9: 102327-102344. Available from: https://doi.org/10.1109/ACCESS.2021.3097559.

[19] Zhang R, Guo Z, Sun Y, Lu Q, Xu Z, Yao Z, et al. COVID-19XrayNet: A two-step transfer learning model for the COVID-19 detecting problem based on a limited number of chest X-Ray images. *Interdisciplinary Sciences: Computational Life Sciences*. 2020; 12(4): 555-565. Available from: https://doi.org/10.1007/s12539-020-00393-5.

[20] Litjens G, Kooi T, Bejnordi BE, Setio AAA, Ciompi F, Ghafoorian M, et al. A survey on deep learning in medical image analysis. *Medical Image Analysis*. 2017; 42: 60-88. Available from: https://doi.org/10.1016/j.media.2017.07.005.

[21] Greenspan H, Van Ginneken B, Summers RM. Guest editorial deep learning in medical imaging: Overview and future promise of an exciting new technique. *IEEE Transactions on Medical Imaging*. 2016; 35(5): 1153-1159. Available from: https://doi.org/10.1109/TMI.2016.2553401.

[22] Roth HR, Lu L, Liu J, Yao J, Seff A, Cherry K, et al. Improving computer-aided detection using convolutional neural networks and random view aggregation. *IEEE Transactions on Medical Imaging*. 2016; 35(5): 1170-1181. Available from: https://doi.org/10.1109/TMI.2015.2482920.

[23] Tajbakhsh N, Shin JY, Gurudu SR, Hurst RT, Kendall CR, Gotway MB, et al. Convolutional neural networks for medical image analysis: Full training or fine tuning? *IEEE Transactions on Medical Imaging*. 2016; 35(5): 1299-1312. Available from: https://doi.org/10.1109/TMI.2016.2535302.

[24] Mikołajczyk A, Grochowski M. Data augmentation for improving deep learning in image classification problem. In: *2018 International Interdisciplinary PhD Workshop (IIPhDW)*. Świnoujście, Poland: IEEE; 2018. p.117-122. Available from: https://doi.org/10.1109/IIPHDW.2018.8388338.

[25] Mahase E. Coronavirus: Covid-19 has killed more people than SARS and MERS combined, despite lower case fatality rate. *BMJ*. 2020; 368: m641. Available from: https://doi.org/10.1136/bmj.m641.

[26] Wang W, Xu Y, Gao R, Lu R, Han K, Wu G, et al. Detection of SARS-CoV-2 in different types of clinical specimens. *JAMA*. 2020; 323(18): 1843-1844. Available from: https://doi.org/10.1001/jama.2020.3786.

[27] Corman VM, Landt O, Kaiser M, Molenkamp R, Meijer A, Chu DK, et al. Detection of 2019 novel coronavirus (2019-nCoV) by real-time RT-PCR. *Eurosurveillance*. 2020; 25(3): 2000045. Available from: https://doi.org/10.2807/1560-7917.ES.2020.25.3.2000045.

[28] Lal A, Mishra AK, Sahu KK. CT chest findings in coronavirus disease-19 (COVID-19). *Journal of the Formosan Medical Association*. 2020; 119(5): 1000-1001. Available from: https://doi.org/10.1016/j.jfma.2020.03.010.

[29] Fang Y, Zhang H, Xie J, Lin M, Ying L, Pang P, et al. Sensitivity of chest CT for COVID-19: Comparison to RT-PCR. *Radiology*. 2020; 296(2): E115-E117. Available from: https://doi.org/10.1148/radiol.2020200432.

[30] Xie X, Zhong Z, Zhao W, Zheng C, Wang F, Liu J. Chest CT for typical coronavirus disease 2019 (COVID-19) pneumonia: Relationship to negative RT-PCR testing. *Radiology*. 2020; 296(2): E41-E45. Available from: https://doi.org/10.1148/radiol.2020200343.

[31] Thepade SD, Chaudhari PR, Dindorkar MR, Bang SV. COVID-19 identification using machine learning classifiers with histogram of luminance chroma features of chest X-Ray images. In: *2020 IEEE Bombay Section Signature Conference (IBSSC)*. Mumbai, India: IEEE; 2020. p.36-41. Available from: https://doi.org/10.1109/IBSSC51096.2020.9332160.

[32] Qjidaa M, Mechbal Y, Ben-fares A, Amakdouf H, Maaroufi M, Alami B, et al. Early detection of COVID-19 by deep learning transfer model for populations in isolated rural areas. In: *2020 International Conference on Intelligent Systems and Computer Vision (ISCV)*. Fez, Morocco: IEEE; 2020. p.1-5. Available from: https://doi.org/10.1109/ISCV49265.2020.9204099.

[33] Darapaneni N, Ranjane S, Satya USP, Prashanth DK, Reddy MH, Paduri AR, et al. COVID-19 severity of pneumonia analysis using chest X-Rays. In: *2020 IEEE 15th International Conference on Industrial and Information Systems (ICIIS)*. Rupnagar, India: IEEE; 2020. p.381-386. Available from: https://doi.org/10.1109/ICIIS51140.2020.9342702.

[34] Shankar K, Perumal E, Tiwari P, Shorfuzzaman M, Gupta D. Deep learning and evolutionary intelligence with fusion-based feature extraction for detection of COVID-19 from chest X-Ray images. *Multimedia Systems*. 2022; 28: 1175-1187. Available from: https://doi.org/10.1007/s00530-021-00800-x.

[35] Shastri S, Singh K, Kumar S, Kour P, Mansotra V. Deep-LSTM ensemble framework to forecast Covid-19: An insight to the global pandemic. *International Journal of Information Technology*. 2021; 13(4): 1291-1301. Available from: https://doi.org/10.1007/s41870-020-00571-0.

[36] Goodfellow I, Pouget-Abadie J, Mirza M, Xu B, Warde-Farley D, Ozair S, et al. Generative adversarial networks. *Communications of the ACM*. 2020; 63(11): 139-144. Available from: https://doi.org/10.1145/3422622.

[37] Kora Venu KS, Ravula S. Evaluation of deep convolutional generative adversarial networks for data augmentation of chest X-Ray images. *Future Internet*. 2021; 13: 8. Available from: https://doi.org/10.3390/fi13010008.

[38] PM. *Chest X-Ray pneumonia*. Available from: https://github.com/ieee8023/covid-chestxray-dataset [Accessed January 2022].

[39] Cohen JP, Morrison P, Dao L. COVID-19 image data collection. *arXiv:2003.11597*. 2020. Available from: https://doi.org/10.48550/arXiv.2003.11597.

[40] Hitawala S. Comparative study on generative adversarial networks. *arXiv:1801.04271*. 2018. Available from: https://doi.org/10.48550/arXiv.1801.04271.

[41] Basori AH, Malebary SJ, Alesawi S. Hybrid deep convolutional generative adversarial network (DCGAN) and Xtreme gradient boost for X-Ray image augmentation and detection. *Applied Sciences*. 2023; 13: 12725. Available from: https://doi.org/10.3390/app132312725.

[42] Ahmadinejad M, Ahmadinejad I, Soltanian A, Mardasi KG, Taherzade N. Using new technique in sigmoid volvulus surgery in patients affected by COVID-19. *Annals of Medicine and Surgery*. 2021; 70: 102789. Available from: https://doi.org/10.1016/j.amsu.2021.102789.

[43] Liu B, Lv J, Fan X, Luo J, Zou T, Kumar M. Application of an improved DCGAN for image generation. *Mobile Information Systems*. 2022; 2022: 9005552. Available from: https://doi.org/10.1155/2022/9005552.

[44] Wu J. *Introduction to convolutional neural networks*. Available from: https://cs.nju.edu.cn/wujx/paper/CNN.pdf [Accessed 10th September 2025].

[45] Chollet F. Xception: Deep learning with depthwise separable convolutions. In: *2017 IEEE Conference on Computer Vision and Pattern Recognition (CVPR)*. Honolulu, HI, USA: IEEE; 2017. p.1800-1807. Available from: https://doi.org/10.1109/CVPR.2017.195.

[46] Oyedele O. Determining the optimal number of folds to use in a K-fold cross-validation: A neural network classification experiment. *Research in Mathematics*. 2023; 10(1): 2201015. Available from: https://doi.org/10.1080/27684830.2023.2201015.

[47] Tabik S, Gómez-Ríos A, Martín-Rodríguez JL, Sevillano-García I, Rey-Area M, Charte D, et al. COVIDGR dataset and COVID-SDNet methodology for predicting COVID-19 based on chest X-Ray images. *IEEE Journal of Biomedical and Health Informatics*. 2020; 24(12): 3595-3605. Available from: https://doi.org/10.1109/JBHI.2020.3037127.

[48] Shuja J, Alanazi E, Alasmary W, Alashaikh A. COVID-19 open source data sets: A comprehensive survey. *Applied Intelligence*. 2021; 51(3): 1296-1325. Available from: https://doi.org/10.1007/s10489-020-01862-6.

[49] Narin A. Detection of Covid-19 patients with convolutional neural network based features on multi-class X-Ray chest images. In: *2020 Medical Technologies Congress (TIPTEKNO)*. Antalya, Turkey: IEEE; 2020. p.1-4. Available from: https://doi.org/10.1109/TIPTEKNO50054.2020.9299289.

[50] Ohata EF, Bezerra GM, Das Chagas JVS, Neto AVL, Albuquerque AB, De Albuquerque VHC. Automatic detection of COVID-19 infection using chest X-Ray images through transfer learning. *IEEE/CAA Journal of Automatica Sinica*. 2021; 8(1): 239-248. Available from: https://doi.org/10.1109/JAS.2020.1003393.

[51] Al-Waisy AS, Al-Fahdawi S, Mohammed MA, Abdulkareem KH, Mostafa SA, Maashi MS, et al. RETRACTED ARTICLE: COVID-CheXNet: Hybrid deep learning framework for identifying COVID-19 virus in chest X-Rays images. *Soft Computing*. 2023; 27: 2657-2672. Available from: https://doi.org/10.1007/s00500-020-05424-3.

[52] Ibrahim AU, Ozsoz M, Serte S, Al-Turjman F, Yakoi PS. Pneumonia classification using deep learning from chest X-Ray images during COVID-19. *Cognitive Computation*. 2024; 16: 1589-1601. Available from: https://doi.org/10.1007/s12559-020-09787-5.